



# Modeling of shrinkage during investment casting of thin-walled hollow turbine blades<sup>☆</sup>



Y.W. Dong<sup>a,b,c,\*</sup>, X.L. Li<sup>a</sup>, Qi Zhao<sup>a</sup>, Jun Yang<sup>c</sup>, Ming Dao<sup>c</sup>

<sup>a</sup> School of Aerospace Engineering, Xiamen University, 422 South Siming Road, Xiamen 361005, PR China

<sup>b</sup> Shenzhen Research Institute, Xiamen University, No. 19, Gaoxin South 4th Road, Nanshan District, Shenzhen 518057, PR China

<sup>c</sup> Department of Materials Science and Engineering, Massachusetts Institute of Technology, Cambridge, 77 Massachusetts Avenue, Cambridge, MA 02139, USA

## ARTICLE INFO

### Article history:

Received 25 July 2016

Received in revised form 8 January 2017

Accepted 9 January 2017

Available online 18 January 2017

### Keywords:

Dimensional shrinkage

Structural identification

Deformation decoupling

Hollow turbine blade

Investment casting die

## ABSTRACT

The shrinkage ratio is a key parameter in designing the investment casting die for hollow turbine blades of high-performance aircraft engines. To avoid extensive modifications to the die shape, we took a single-crystal hollow turbine blade as the typical part to determine the nonuniform shrinkage distribution while considering its structural characteristics during investment casting. By using the structural identification method, different geometrical structures were identified, and the displacement field was established and verified via numerical prediction and experimental measurement. The deformation characteristics, including the wall-thickness distribution and shrinkage ratio, can be established by deformation decoupling analysis. The optimized die profile designed on the basis of the calculation results is in good agreement with the investment casting die in actual use, which indicates that the proposed method is beneficial for improving the geometrical accuracy of hollow turbine blades.

© 2017 Elsevier B.V. All rights reserved.

## 1. Introduction

Investment casting is usually adopted for producing high-quality parts having intricate shapes, owing to its ability to provide multiple degrees of freedom in design, as well as thin-walled components requiring good surface finish and a high degree of dimensional tolerance, such as gas turbine blades, which operate under extreme and complex environmental conditions. However, investment casting involves multiple nonlinear physical processes, which require consideration of geometry, material properties, and boundary conditions, as well as several complicated phenomena such as high-temperature sintering of ceramics, directional solidification of superalloys, and coupling characteristics of complex structure and materials. Accordingly, there is a constant need for methods that can be used to predict the final cast shape and control the cast dimensions with an appropriate degree of accuracy.

Despite the fact that the geometry information of the investment cast can be acquired from the design specifications directly, however, during investment casting, the produced cast dimensions are smaller than those of the die cavity because of wax shrinkage and alloy material solidification. Furthermore, the shape of the cast heavily relies upon the geometry of the metal die cavity. Therefore, it is essential to develop a method for controlling the cast dimensions and improving the quality of the net-shape products while considering the various shrinkages generated during the casting process. However, the fabrication of turbine blades by investment casting is a very complex process, and the shrinkage during casting is highly nonlinear. Hence, it is necessary to determine the deformation and the distribution of cast shrinkages during the solidification process.

Numerous researchers have investigated dimensional changes during investment casting using various types of advanced measurement equipment. Zhang et al. (2010) and Jiang and Liu (2007) used a coordinate measurement machine (CMM) to determine the cast deformation. Yunyong et al. (2014) investigated the geometrical shape of investment turbine blades via multi-source digital measurement; actual data were measured using a CMM and the Advanced Topometric Sensor (ATOS). Wang et al. (2013) investigated the influence of the process parameters on the cavity pressure and dimensional variations of the wax patterns using a commercial simulation code and experimental data

<sup>☆</sup> The authors are grateful for the financial support provided by the PhD Start-up Fund of Natural Science Foundation of Guangdong Province (2014A030310004), the Major Science and Technology Project between University-Industry Cooperation in Fujian Province (2015H6023), and the China Scholarship Council.

\* Corresponding author at: School of Aerospace Engineering, Xiamen University, 422 South Siming Road, Xiamen 361005, PR China.

E-mail address: [yiwei.mit@gmail.com](mailto:yiwei.mit@gmail.com) (Y.W. Dong).

obtained by a three-dimensional laser scanner. Liu et al. (2015) used a three-dimensional (3D) scanner and an industrial computerized tomography (ICT) scanner to study the influence of complex structure on part shrinkage in the investment casting process. Furthermore, in recent years, several researchers have used other nondestructive testing methods, such as ultrasonic, shearography, and thermography techniques, for the inspection and measurement of turbine blades. Thus, high-precision turbine blade measurement has been achieved by using various types of advanced measurement methods and complicated instruments.

With the ever-increasing sophistication of computer hardware and software, computer simulation of casting is becoming more accessible (Khan and Sheikh, 2016). Researchers have used extensively large-scale finite element analysis software in die profile design optimization and deformation prediction during the casting process. Norouzi et al. (2009) simulated the residual stresses and hot tearing in investment casting using the MAGMA simulation package. Afazov et al. (2011) developed a simulation package that can predict the residual stresses in the bottom core vane (BCV) component of an aircraft engine in the circumstances of equiaxed cooling on the basis of the finite element method (FEM). Aveson et al. (2013) confirmed the occurrence of high stresses in constricted channels where sliver defects originate in seeded single-crystal form. Hang et al. (2014) simulated and optimized the directional solidification process of single-crystal superalloy blade samples on the basis of the cellular automaton-finite difference (CA-FD) method. Chattopadhyay (2011) established a method for estimating the solidification time in investment casting by building a functional relationship between the solidification time obtained from lumped analysis and the full-phase complete solution of the energy equation. From previous studies, it can be concluded that solidification simulation has been widely used to predict residual stress and shrinkage during investment casting. Several commercial software suites, such as ProCAST (ESI Group, Paris, France), ANSYS (ANSYS, Inc., Canonsburg, Pennsylvania, United States), and ABAQUS (Dassault Systèmes, Vélizy-Villacoublay, France), have been employed to investigate and optimize the casting process.

Given the stringent tolerance requirements for turbine blades, there is a constant need to better understand and further improve the investment casting die profile design in terms of casting accuracy and consistency. The establishment of the die profile is currently based on the linear scaling (LS) method. The LS method, which is simple and neutral, uses a constant shrinkage ratio to design the profile. Realistically, owing to the influence of casting structures and various constraints, the shrinkage distribution is inhomogeneous. Therefore, determining the nonuniform shrinkage requires improved geometrical accuracy of the die profile.

Sabau (2006) adopted a method that uses different shrinkage rates for different directions; however, the shrinkage rate remains constant along each coordinate axis in their method. Modukuru et al. (1996) proposed a grid-displacement reverse-stacking method for designing the die profile, whereby the calculated deformations are reversed and stacked into each node. Nevertheless, accurate boundary conditions, which are required to achieve high accuracy in numerical modeling, are difficult to establish. Dong et al. (2011b) proposed a spring-back compensation method that measures the displacement field of the part and adjusts the cavity shape on the basis of geometrical parameters. However, the coupling effect of shrinkage and the complex structure of thin-walled hollow turbine blades have not been considered in existing studies.

Here we propose a simple yet accurate method to determine the shrinkage ratio while considering the structural characteristics of thin-walled hollow turbine blades during investment casting. This method is useful for effectively designing the investment die profile of hollow turbine blades. The die profile designed on the

basis of the proposed shrinkage model is expected to significantly improve the quality of the produced turbine blades.

## 2. Development of the structure identification method

Owing to the complexity of the outer and inner shapes of hollow turbines, the cast deformation depends on the integrated operation of many factors (Liu et al., 2015). The cast deformation is closely related not only to the properties of materials having unstable compositions but also to the casting structure and forming conditions.

Specifically, under certain process conditions and material compositions, the deformation is closely related to the structural and geometrical characteristics of the cast. Take the hollow turbine blade for example; the airfoil cross section of the hollow turbine blade is shown in Fig. 1. As shown in Fig. 1, the methods for calculating the deformation of points  $P_1$  and  $P_2$  are different. Owing to the restriction effect of the ceramic core,  $P_1$  is subjected to restriction by the ceramic core when the metal solidifies and cools, whereas  $P_2$ 's solidification is unrestrained. Therefore, each point on the cross section exhibits different deformation behavior. Given that the structural characteristics of the hollow turbine blade are essential for determining the deformation, accurate structural identification is necessary.

### 2.1. Determination of section parameters

In general, the geometrical parameters of the turbine blade can be acquired by means of measurement. They can also be determined using commercially developed solidification simulation software based on finite element analysis. The geometrical data obtained can be represented in the STL (STereoLithography) format, a file format that is widely used for rapid prototyping and computer-aided manufacturing.

Blades 1 and 2 shown in Fig. 2 represents two types of hollow turbine blades. As depicted in Fig. 2, there are three types of typical structures: the deformation-restrained (DR) structure, the non-restrained (NR) structure, and the intersecting (IS) structure. Area  $\alpha$  represents the DR structure; this type of structure will be restrained while deforming. The areas including point  $\beta$  and its neighboring structures, as shown in Fig. 2, depict the NR structure; this structure can be deformed freely and will not be restricted by the ceramic core. Area  $\gamma$  represents the cooling configuration for the trailing edge of the turbine blade and represents the IS structure. The IS structure occurs only at the trailing edge, where no reliable means of measurement is available. Additionally, the IS structure is not a universal structural characteristic of a hollow turbine blade, and the DR and NR structures can be used for describing the main types of structural characteristics. Therefore, to simplify the method for identifying the structural characteristics of a hollow turbine blade, the  $\gamma$ -type IS structure is not discussed in this paper.

In general, the obtained point cloud data of the hollow turbine blade can be quite complex. The STL format is widely used for representing complex 3D models. The point cloud data obtained via measurements and simulation are transformed into the STL format. The cross-sectional data can be intercepted by the plane from the casting model.

As shown in Fig. 3(a), the cross-sectional data constitute a set of discrete points; this set needs to be reconstructed to establish the contour profile. To ensure contour fairness, an algorithm based on the least-squares estimation of B-splines is used for fitting the discrete points.

The B-spline equation can be expressed as (Zhao et al., 2011)

$$P(u) = \sum_{i=1}^n d_i N_{i,k}(u), \quad (1)$$

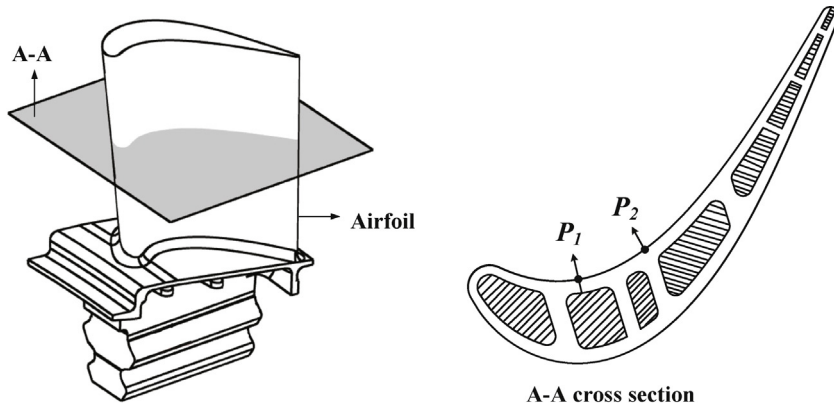


Fig. 1. Schematic of the turbine blade and a cross section of its hollow structure.

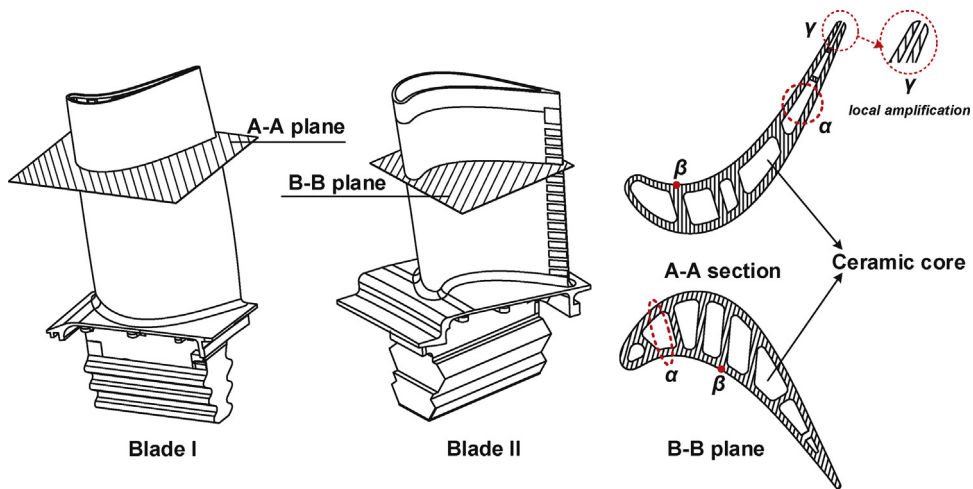


Fig. 2. Structural characteristics of the hollow turbine section.

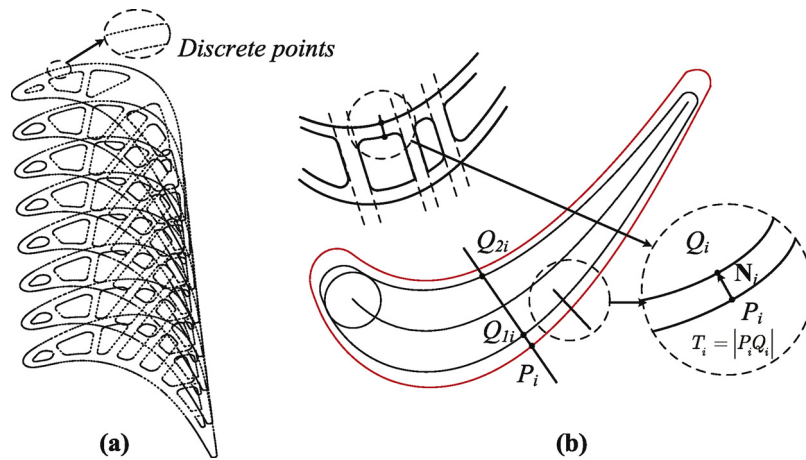


Fig. 3. Schematic showing the definition of wall thickness.

where the basis functions  $N_{i,k}(u)$  are given by

$$N_{i,k}(u) = \begin{cases} 1, & x_i < t < x_{i+1}, \\ 0, & \text{otherwise,} \end{cases} \quad (2)$$

$$N_{i,k}(u) = \frac{(u - x_i)N_{i,k-1}(u)}{x_{i+k-1} - x_i} + \frac{(x_{i+k} - u)N_{i+1,k-1}(u)}{x_{i+k} - x_i}, \quad (3)$$

where  $x_i$  are the elements of an open knot vector  $[\mathbf{X}]$ ,  $k$  is the order of the B-spline basis function,  $u$  is the spline parameter, and  $n$  represents the number of defining polygon points. The knot vector of the polygon points can be parameterized by the method of accumulating chord length (Bergstrom, 2015):

$$\bar{u}_i = \frac{1}{L} \sum_{j=1}^i l_j, \quad i = 1, 2, \dots, m - 1, \quad (4)$$

where  $l_i = \{ |q_i - q_{i-1}| \}$  after normalization,  $\bar{u}_0 = 0$ , and  $\bar{u}_m = 1$ . Repeating the knots at the end  $k$  times can force the endpoints to coincide with the control polygon. For the reconstruction of the cross-sectional data,  $k = 3$  can meet the requirement of fitting accuracy and efficiency. If the point set  $P = \{p_j : j = 1, 2, \dots, r\}$  belongs to the fitting curve, the following relational equation should be met:

$$P_j(u_i) = \sum_{i=0}^n d_i N_{i,k}(u_j), \quad j = 1, 2, \dots, r, \quad (5)$$

where  $k < n < r$ . Note that Eq. (5) is a restricted equation, and its approximate solution can be obtained by the least-squares fitting method. The objective function can be expressed as

$$E = \sum_{i=0}^N \|r(u_i) - P_i\|^2. \quad (6)$$

When  $E \rightarrow \min$ ,  $d = (\mathbf{N}^T \mathbf{N})^{-1} \mathbf{N}^T \mathbf{P}$  can be determined. Then, the B-spline approximation based on least squares can be acquired.

There exist significant differences in shrinkage determination between the DR and NR structures, which mainly originate from the calculated wall thickness of the hollow structure. The wall thickness can be defined as follows. For any point on the profile of the castings,  $M_i (i = 1, 2, \dots, n)$ , consider  $\mathbf{N}_i$  as the normal direction of the point,  $M_i$  as the starting point,  $Q_i$  as the intersection point of the vector direction and the inner surface, and  $T_i$  as the distance between points  $P_i$  and  $Q_i$ . Then,  $T_i$  can be regarded as the wall thickness at point  $P_i$ , as shown in Fig. 3(b).

The calculated wall thickness can be deemed as the distance of the intersection points between the intersecting line and the curve, as shown in Fig. 3(b). The algorithm can be described as follows: If one assumes that the outer contour of the cross section  $C_\omega(\mu)$  is dispersed into  $n$  points, denoted by  $P_i (i = 1, 2, \dots, n)$ , the unit normal vector along the inner normal direction at each point is  $N_i (i = 1, 2, \dots, n)$ , where point  $P_i$  is the starting point and  $N_i$  is the direction vector. Line  $L$  can be constructed as

$$L_i = P_i + tN_i \quad (i = 1, 2, \dots, n). \quad (7)$$

The parametric equation for constructing the inner profile of the cross section is given by

$$\mathbf{r} = \mathbf{r}(\mu). \quad (8)$$

The intersection points of line  $L_i$  and inner profiles  $Q_{1i}$  and  $Q_{2i}$  are determined by Eqs. (7) and (8). By definition,  $T_i = |P_i Q_{1i}|$  is the wall thickness.

### 2.2. Section structural identification

Next, the DR and NR structures need to be identified. The threshold method was used to identify the structural characteristics. The absolute value of the wall-thickness difference between two adjacent points on the cross section,  $P = |y_{i+1} - y_i|$ , was chosen as the criterion. Given  $\Delta D$  as the threshold value, if  $\Delta D \leq P$ ,  $tag = 0$  and otherwise,  $tag = 1$ , where  $tag$  is the identifier. Note that  $tag = 1$  implies that the structure is changed, whereas  $tag = 0$  implies that the structure remains unchanged. To improve the identification efficiency and accuracy, and to reduce the sensitivity of the identified criterion owing to the use of a single threshold value, the ascending power method was used. Let  $i = x_i$ , where  $i$  represents the sequence number of the discrete points on the cross section. Let  $y_i$  be the corresponding wall thickness of point  $x_i$ ; hence, the one-dimensional data  $y_i$  can be transformed into two-dimensional data  $(x_i, y_i)$ , which can be regarded as a point on the plane. Accordingly, a triangle  $S_i$  can be formed by  $(x_i, y_i)$  and the adjacent points  $(x_{i-1}, y_{i-1})$  and

**Table 1**

Wall thickness of chosen points based on the structural identification algorithm and comparison with actual data.

Point	Actual wall thickness	Identification result	Deviation
A	4.2412	4.22424	0.001696
B	1.6637	1.66295	0.000750
C	1.6780	1.69664	-0.018637
D	0.9045	0.90149	0.003010
E	2.2546	2.26466	-0.010060
F	1.8405	1.84605	-0.005550

$(x_{i+1}, y_{i+1})$ . The area of the triangle can be calculated using Heron's formula based on the lengths of the sides.

In single-structural areas such as the DR and NR areas, the change in the triangle vertex follows a consistent trend. Consequently, the triangle constructed is small. However, in areas of drastic structural change, owing to the change in wall thickness, the area of the triangle will increase significantly. Therefore, given a certain triangular area, the improved threshold algorithm can be described as follows:

1. Calculate the area of each triangle, denoted by  $S_i$ . Compare all  $S_i$  and sort them in ascending order as  $\{S_j\}_{des}$ .
2. Calculate the error between two adjacent values in  $\{S_j\}_{des}$  sequentially, denoted by  $\{\Delta S_j\}$ .
3. Compare  $\{\Delta S_j\}$  and the given threshold value  $\Delta D$ . If  $\{\Delta S_j\} \neq 0$  and  $\{\Delta S_j\} < \Delta D$ , set  $\Delta D = \{\Delta S_j\}$ .

With the determination of the threshold value, and under the assumption that the identifier  $tag$  of the start point  $i = 0$  is known, the structural identification algorithm can be described as follows:

1. The identifier  $tag$  is given.
2. Calculate the area of the triangle formed by three adjacent points  $S_i$ .
3. Given the threshold value  $\Delta D$ , if  $\Delta D < S_i$ , the value of  $tag$  remains constant; otherwise, let  $tag = 1$ . The change value represents the wall thickness of the NR structure.

The procedure of the algorithm is shown in Fig. 4.

### 2.3. Verification of identification algorithm

To verify the accuracy of the structural identification algorithm, six points representing different structural types on both suction and pressure sides of the turbine blade cross section were chosen, as shown in Fig. 5. Points A and E represent the NR structure, points B and C represent the DR structure, and points D and F represent the transitional phase between the two structural types.

The actual wall thickness of each point was determined using UG NX7™ (Siemens PLM Software, Munich, Germany), based on the structural identification algorithm described in Sections 2.1 and 2.2. The calculated wall thickness values are listed in Table 1.

From Table 1, we can conclude that, based on the identification algorithm, different structural types can be identified successfully. The deviations of the wall thicknesses of the chosen points are relatively small, which proves that the proposed algorithm facilitates satisfactory structural identification of hollow turbine blades.

### 3. Shrinkage modeling of thin-walled hollow turbine blades

To create the shrinkage model, it is important to establish the deformation of the thin-walled hollow turbine blade during the solidification process, which is also known as the displacement field. However, the displacement field of such thin-walled hollow

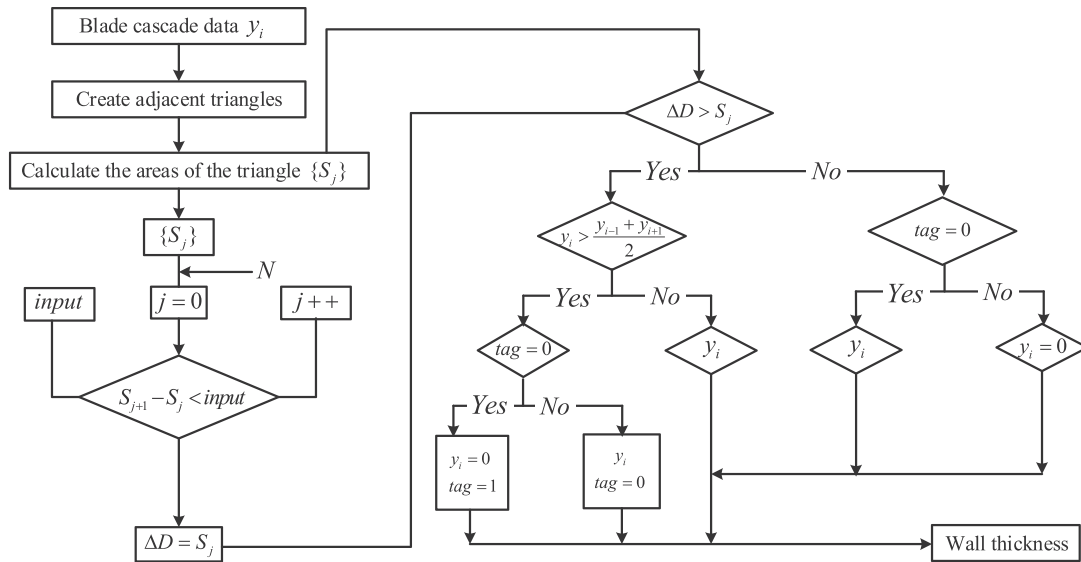


Fig. 4. Flowchart of the triangular area algorithm.

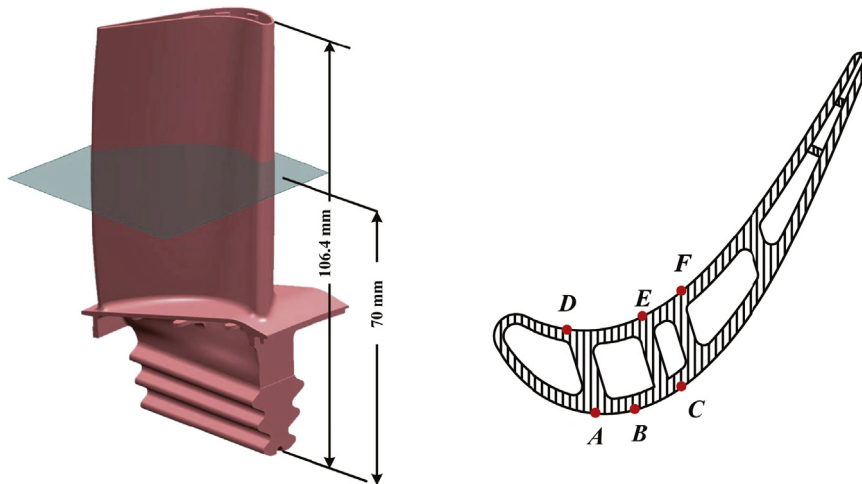


Fig. 5. Locations of the chosen points for identification verification.

structural components often includes different deformation characteristics such as shrinkage, torsion, and bending. This is primarily because of the nonuniform thermal stress induced by different cooling rates generated by complex structures. Hence, it is essential to establish the displacement field and separate the deformation characteristics.

The deformation of turbine blade casts can be obtained by means of numerical simulation or measurement. For any point on the surface of the casting, the total displacement  $D_i$  can be described as

$$D_i = D_{si} + D_{bi} + D_{ti} + D_{ri}, \tag{9}$$

where  $D_{si}$ ,  $D_{bi}$ ,  $D_{ti}$ , and  $D_{ri}$  represent the deformation characteristics of shrinkage, bending, torsion, and random error, respectively. Random errors are induced by measurement, and they can be eliminated by statistical averaging. Thus, Eq. (9) can be rewritten as

$$D_i = D_{si} + D_{bi} + D_{ti}. \tag{10}$$

### 3.1. Decoupling of torsional deformation

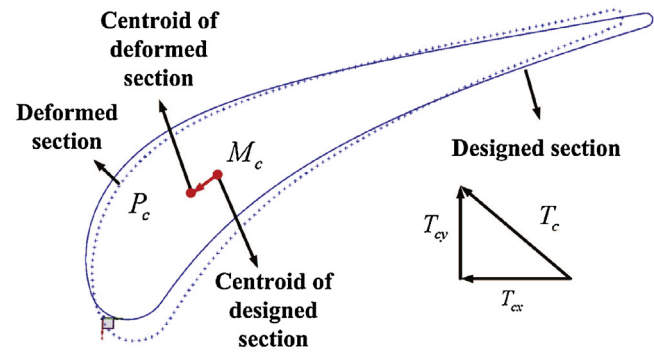
Based on slice processing of the designed and deformed models, a series of two-dimensional (2D) sections of the turbine blade can be obtained, as shown in Fig. 6(b). If we assume that the

torsional deformation has no effect on the sectional geometry, then the 2D cross sections can be regarded as rigid bodies, and each point on the section has the same displacement. Hence, the geometrical centroid of each section was chosen because the centroid location is relatively stable under changes in the discrete points. Therefore, the displacement of the geometrical centroid between the designed model and the deformed model can be considered as the torsional deformation  $D_{ti}$ .

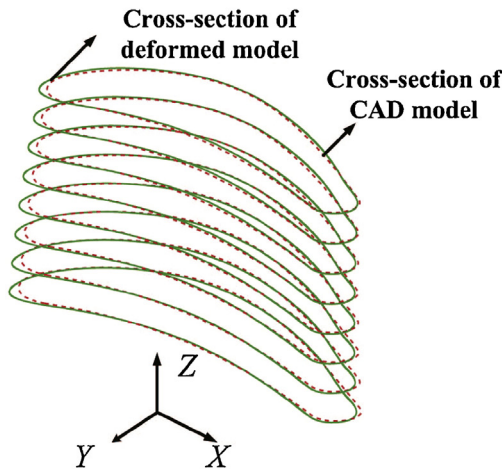
Given the set of discrete points of the sectional contour  $\{p_1, p_2, \dots, p_n\}$ , let  $p_i(x_i, y_i, z_i)$  be the coordinates of the discrete points,  $i = 1, 2, \dots, n$ , and let  $M$  be the geometrical centroid of  $p_i$ , which can be determined as

$$M = \left( \frac{1}{n} \sum_{i=1}^n x_i, \frac{1}{n} \sum_{i=1}^n y_i, \frac{1}{n} \sum_{i=1}^n z_i \right). \tag{11}$$

As shown in Fig. 6(a),  $P_c$  and  $M_c$  denote the cross-sectional geometrical centroids of the designed and deformed models, respectively. Let  $T_c = (T_{cx}, T_{cy}, 0)$  be the centroid displacement. Each point on the same section with the same height has the same deformation characteristics; thus,  $D_{ti} = T_c$ . Owing to the changing solidification conditions and cooling rates, different sections with



(a) Torsional deformation of a cross section at a given position



(b) Cross sections of the turbine blade

Fig. 6. Schematic of the torsional deformation of the turbine blade.

different heights have different torsional deformations. To analyze the shrinkage deformation, the torsional deformation should be eliminated from the displacement field. Based on the inverse design method, the torsional deformation  $D_{ti}$  can be compensated by

$$P'_i = P_i + D_{ti}, \tag{12}$$

where  $P_i$  and  $P'_i$  represent any point on the surface of the deformed model and the point on the model without torsional deformation, respectively. Hence, we have  $P'_c = P_c + D_{ti}$ , where  $P_c$  and  $P'_c$  represent the geometrical centroid of the deformed model

and the geometrical centroid of the model without torsional deformation, respectively. Theoretically, the geometrical centroid of the designed section  $M_c$  and that of the deformed section  $P'_c$  coincide, i.e.,  $P'_c = M_c$ , after compensation.

### 3.2. Decoupling of bending deformation

The angular displacement of the deformed model relative to the designed model, expressed by the torsional angle, can be used to represent the bending deformation. With the compensation of the torsional deformation described in Section 3.1, the geometrical centroids of the designed and deformed sections coincide. As shown in Fig. 7, points A and B represent the leading edge points of the deformed and designed sections, respectively. The leading edge is the region where the gas flow first hits the blade. The definitions of the geometrical parameters of the turbine blade cross section are detailed in the work of Dong et al. (2011b). The torsional angle can be described as the angle formed by connecting the geometrical centroid and the leading edge point of the cross section.

In Fig. 7,  $P'_c$  and  $M_c$  coincide after compensation, defining the angle of  $P'_cA$  relative to  $M_cB$  as the torsional angle  $\theta$ , in the positive counterclockwise direction. Thus, the bending deformation can be compensated using a rotational transformation of the points  $P'_i$ . The compensated points  $P''_i$  can be determined by using

$$P''_i = P'_i \cdot R, \tag{13}$$

where  $R$  represents the rotation matrix

$$R = \begin{bmatrix} \cos \theta & -\sin \theta & 0 \\ \sin \theta & \cos \theta & 0 \\ 0 & 0 & 1 \end{bmatrix}. \tag{14}$$

### 3.3. Modeling of shrinkage deformation

The nonlinear and nonuniform shrinkage distribution can be described by a scale coefficient  $K$  as the shrinkage ratio, represented as follows:

$$K = \frac{D - M}{D} \times 100\%, \tag{15}$$

where  $K$  is the shrinkage ratio,  $D$  is the dimension of the die profile, and  $M$  is the dimension of the casting.

As shown in Fig. 8, point  $P_1$  is on the die profile, which changes to  $P_2$  after deformation. Point  $O$  is the center of the maximum inscribed circle corresponding to  $P_2$ . The nonlinear deformation between points  $O_1$  and  $P_2$ , in essence, is the result of the integral operation of the deformation of each point from  $O$  to  $P_2$ , which can

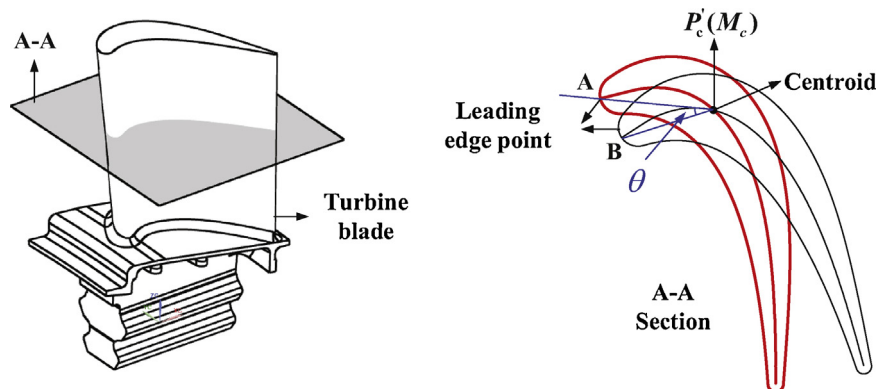


Fig. 7. Schematic of the torsional angle representing the bending deformation of the turbine blade cross section.

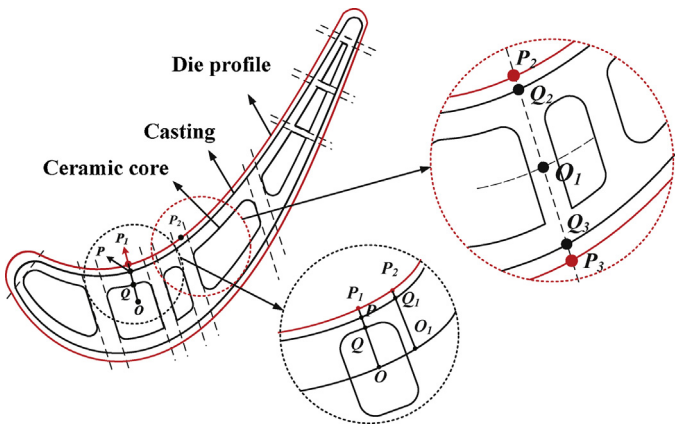


Fig. 8. Schematics of the shrinkage calculation for the hollow structural turbine blade based on its cross section.

be described as

$$\Delta P = \overline{PP_2} = \int_{l=0}^{l=\overline{O_1Q_1}} S_c(x, y, z) \lambda_c(x, y, z) dl + \int_{l=\overline{O_1Q_1}}^{l=\overline{O_1P_2}} S_b(x, y, z) \lambda_b(x, y, z) dl, \quad (16)$$

where  $S_c(x, y, z)$  and  $S_b(x, y, z)$  represent the deformations of the ceramic core and the superalloy caused by the transient temperature field, respectively. Further,  $\lambda_c(x, y, z)$  and  $\lambda_b(x, y, z)$  represent the deformations of the ceramic core and the superalloy that are attributed to the stress field, respectively. Because the casting process is a typical thermo-mechanical coupling process, the thermal deformation can be represented by the deformation induced by the stress field. Let  $\lambda_m$  denote the average strain of the blade thickness  $L$ . According to the definition of shrinkage, the shrinkage ratio  $k$  can be written as

$$k = \frac{\Delta P}{L} = \frac{S_b \left[ \int_{l=\overline{O_1Q_1}}^{l=\overline{O_1P_2}} \lambda_b(x, y, z) dl \right]}{L} = \lambda_m S_b. \quad (17)$$

Simultaneously, given that the materials of the ceramic core are mainly quartz glass substrates and zirconite for high-temperature strength and superior creep resistance, which have near-zero thermal expansion coefficient, it can be assumed that the ceramic core

is not deformed during the casting process; this is denoted as  $S_c(x, y, z) = 0$ .

Therefore, on the macroscopic scale, the shrinkage and the thickness of the material along the shrink direction should be determined to calculate the shrinkage ratio. As shown in Fig. 8, the calculation of the shrinkage ratio for the NR structure can be expressed as

$$S_{P_2} = \frac{\overline{P_2O_1} - \overline{Q_1O_1}}{\overline{P_2Q_1}} \times 100\%. \quad (18)$$

The calculation of the shrinkage ratio for the DR structure can be written as

$$S_{P_1} = \frac{\overline{P_1Q_1} - \overline{PQ}}{\overline{P_1Q_1}} \times 100\%. \quad (19)$$

### 4. Results and discussion

#### 4.1. Displacement field modeling

A high-pressure turbine blade was used in this study. ProCAST was used to model the displacement field during investment casting. The turbine blade, the designed gating system model, and the gating system FEM model as well as their main dimensions are shown in Fig. 9. To improve the computational efficiency, the mesh sizes of the pressure and suction sides, turbine blade body, and gating system were set to 0.1, 0.2, and 2 mm, respectively.

In this study, the as-cast CSX superalloy DD6 was used as the turbine blade casting material. The composition of DD6 is summarized in Table 2. The thermo-physical and mechanical parameters were obtained from Li et al. (2016). Silica sand was used as the shell material; the shell density  $\rho$  is 1520 kg/m<sup>3</sup>, the thermal conductivity is 0.59 W/m/K, and the specific heat capacity is 1.20 kJ/kg/K. The configurations of the process parameters for the simulation were as follows: The initial temperature of the casting, shell, and ceramic core were 1550 °C. The initial temperature of the chill plate was 10 °C. The final temperature for the calculation was 400 °C, i.e., the approximate temperature when the shell mold was removed from the furnace for cooling. The modified interfacial heat transfer coefficients (IHTC) were derived from the finite difference method (FDM) using an explicit technique, which was incorporated into the heat-flow computer program written to estimate the transient IHTC, as

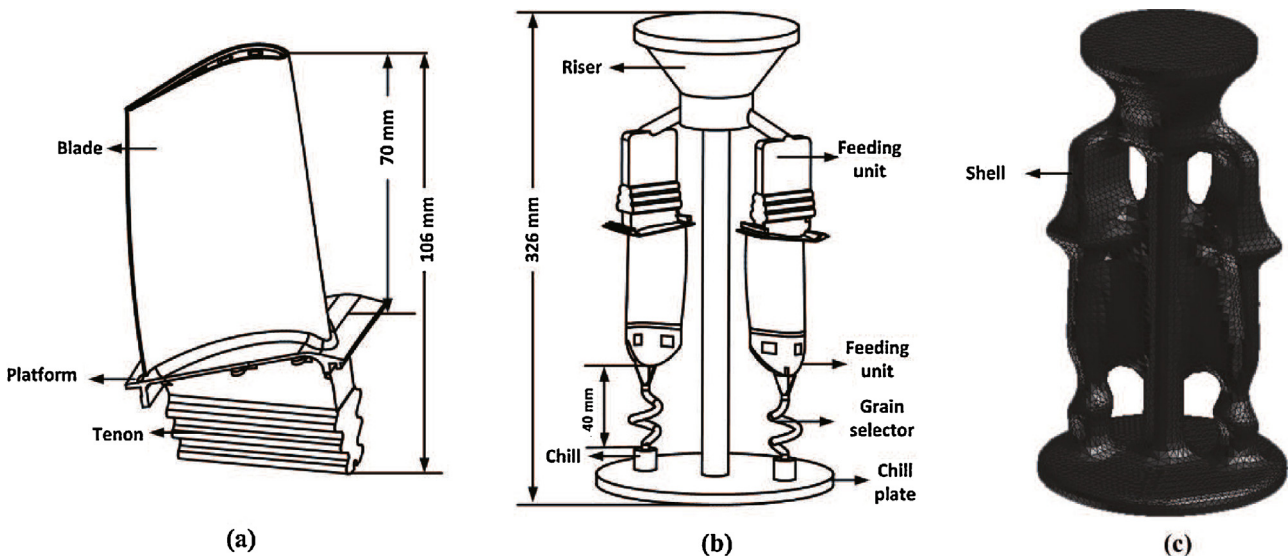


Fig. 9. Model for the displacement field simulation: (a) typical turbine blade, (b) designed gating system model, and (c) gating system FEM model.

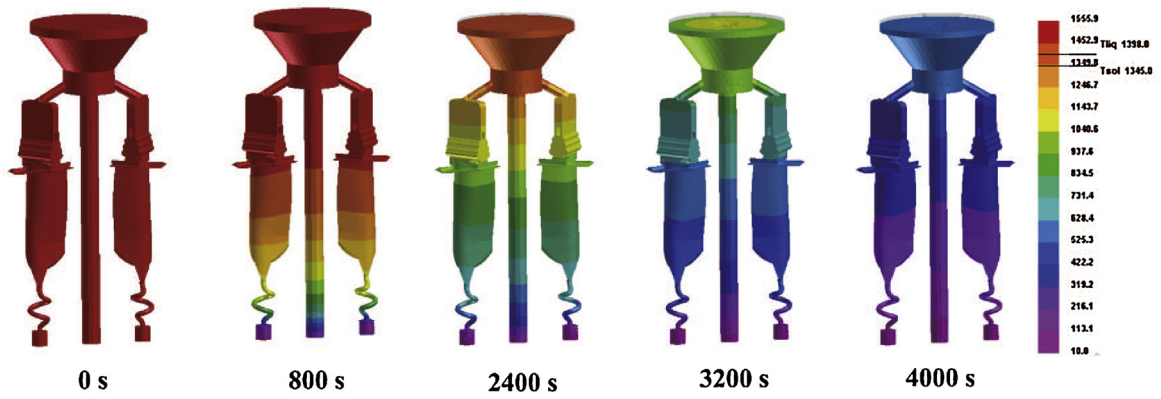


Fig. 10. Time dependence of the temperature field distribution during investment casting.

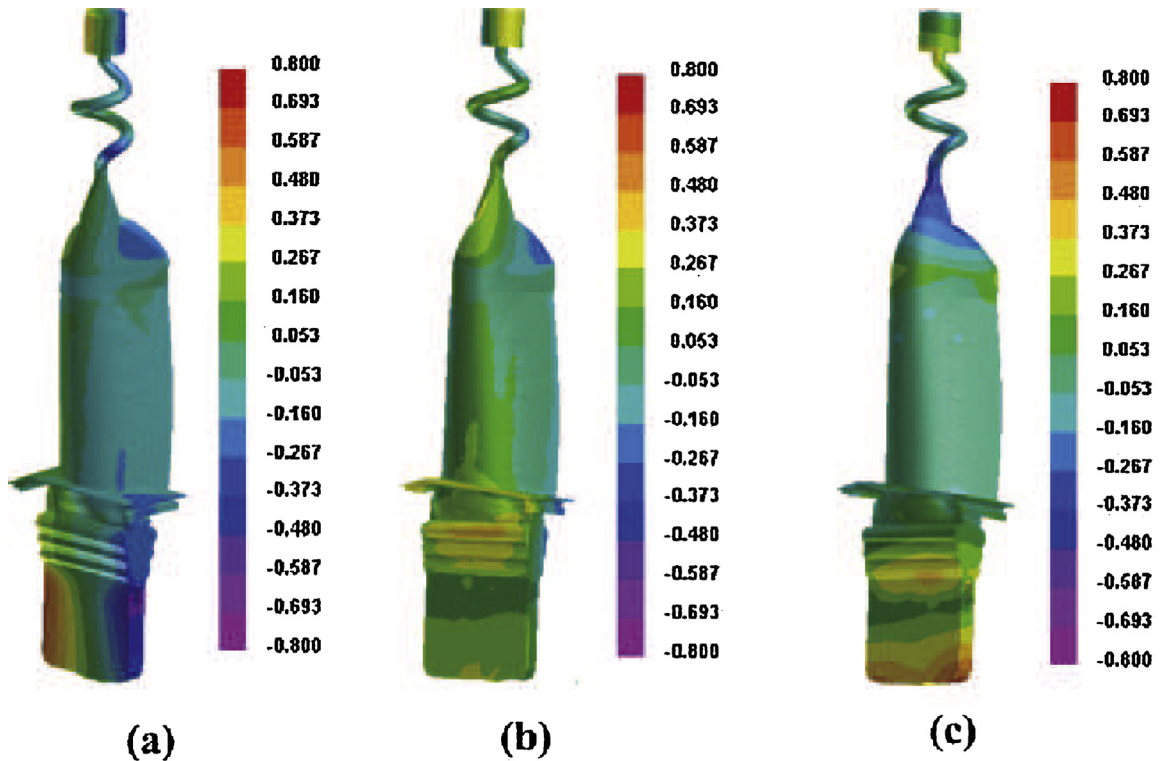


Fig. 11. Distribution of the predicted displacement field in (a) X, (b) Y, and (c) Z directions (in units of millimeters).

Table 2  
Nominal composition of superalloy DD6.

Element	Ni	Cr	Co	Mo	W	Ta	Re	Nb	Al	Hf
wt.%	Balance	4.3	9	2	8	7.5	2	0.5	5.6	0.1

explained in Dong et al. (2011a). Moreover, the solidification process was completed at a withdrawal rate of 4.5 mm/min, with the shell mold fixed in the chill plate.

Fig. 10 shows the simulation results of the time-dependent temperature field distribution of the solidification process (at 0, 800, 2400, 3200, and 4000 s), indicating that the temperature field exhibited a gradient change along the withdrawal direction. Fig. 11(a)–(c) shows detailed views of the final displacement field obtained at the end of the simulation in the X, Y, and Z directions, respectively.

As expected, owing to the coupling effect of the uneven cooling rate and complex structure, the displacement exhibited a nonuni-

form distribution, which can be used to identify and calculate different deformation characteristics.

As shown in Fig. 12, let  $Q(x_Q, y_Q, z_Q)$  be a random point on the designed model, let  $P_0(x_{P_0}, y_{P_0}, z_{P_0})$  be the corresponding point on the deformed casting, and let the XY cross section passing through point  $P_0$  be denoted by  $S(u, v)$ . Further, let  $P_c$  be the projection point of  $Q$  on  $S(u, v)$ , let  $\bar{Q}P_c$  be the minimum distance from point  $Q$  to the cross section, and let  $\mathbf{n}$  be the normal vector to the cross section at point  $P_c$ . Then,  $\bar{Q}P_0$  can be expressed as

$$\bar{Q}P_0 = S_u \Delta u + S_v \Delta v + \mathbf{n} \cdot d, \tag{20}$$

where  $\Delta u$ ,  $\Delta v$ , and  $d$  represent the displacement of point  $Q$  along the X, Y, and Z directions, respectively.

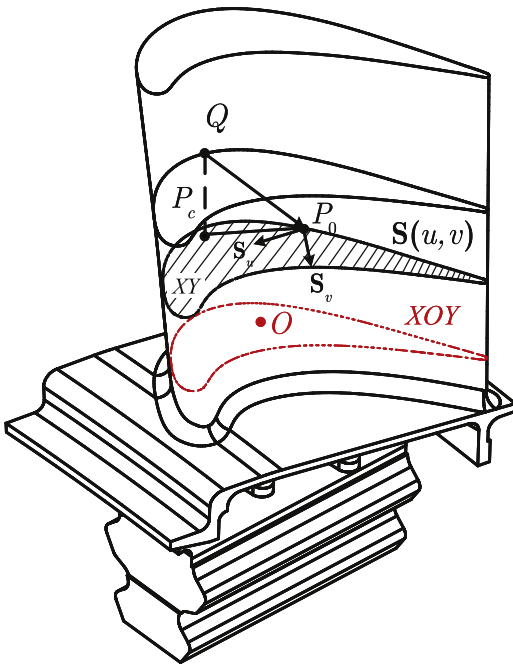


Fig. 12. Displacement field calculation.

According to the shrinkage behavior of the unidirectional solidification, the molten alloy was solidified unidirectionally upward from the chill plate, while the middle part of the casting has the slowest solidification rate based on the Chvorinov principle developed by Chvorinov (1940), which means that the alloy solidified from the outside to the interior. Therefore, the centroid position can be regarded as the shrinkage center of the turbine blade, which has the least deformation of the whole casting. Therefore, the height of cross section  $XOY$  through the centroid point  $O(x_0, y_0, z_0)$  remains constant before and after the investment casting process, and the deformation in the  $Z$  direction is defined by

$$\Delta Z = \mathbf{n} \cdot \mathbf{d} = K_z |z_Q - z_0|, \quad (21)$$

where  $K_z$  represents the shrinkage ratio in the  $Z$  direction, since the deformation along the  $Z$  direction can be decreased or prevented by the feeding unit.  $K_z$  can be regarded as approximately constant.

To establish the displacement field, eight corresponding cross sections at different positions (Fig. 13) were chosen, as shown in Fig. 14. To accommodate the measurement strategy for achieving high measuring accuracy and efficiency by a CMM and to analyze the airfoil section of the turbine blade conveniently, according to the studies of Xiandong et al. (2012) and Wenlong et al. (2014), 200 sampling points from each section were measured. Therefore, the sections were intercepted on the basis of the simulation results and then dispersed into 200 discrete points.

Note that the design of 3D turbine blade is commonly generated by “stacking” 2D sections. It is therefore reasonable to analyze the deformation of the turbine blade based on the 2D sections. To eliminate the effects of using 2D sections, the intercepted cross sections were chosen in equal proportion, which means that the corresponding sections were not at the same height but had the same height proportional ratio relative to the  $XOY$  plane. In addition, to verify the accuracy of the simulated displacement field, a series of hollow turbine blade castings having the same geometrical features was produced by unidirectional solidification. The procedure used is described as follows: Before casting, the solidification furnace was vacuumized to approximately 0.05 Pa, the graphite resistance heating elements of the furnace were used to raise the mold temperature to above the melting point of the alloy,

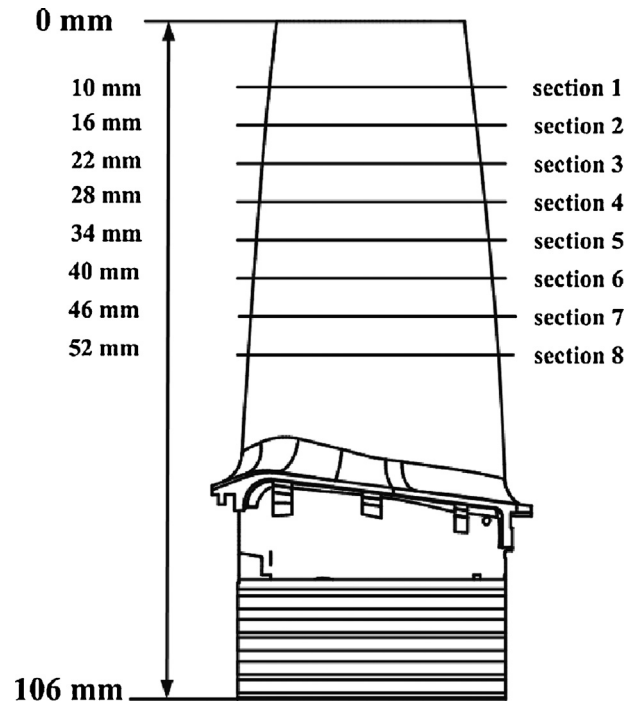


Fig. 13. Positions of the cross sections.

and then the liquid metal was poured into the mold and the mold was placed in the chamber for around 4–5 min to let the liquid metal become stable; the mold was then withdrawn at a rate of 4.5 mm/min. The solidification process was complete in about an

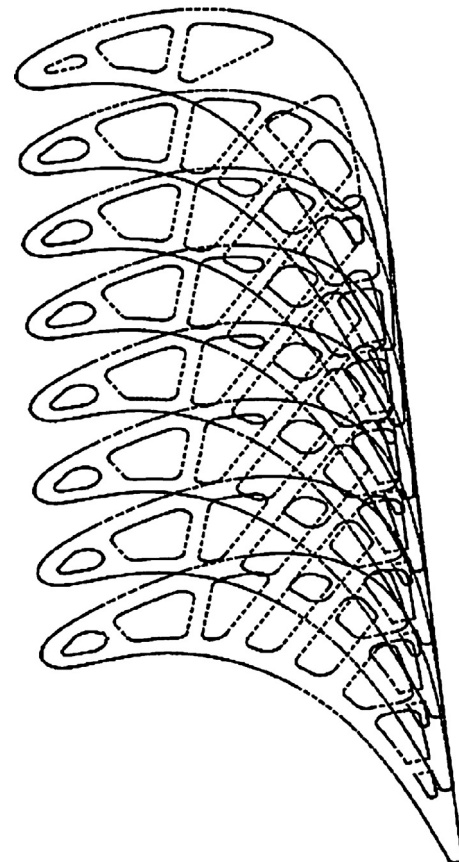


Fig. 14. Cross sections of the turbine blade.

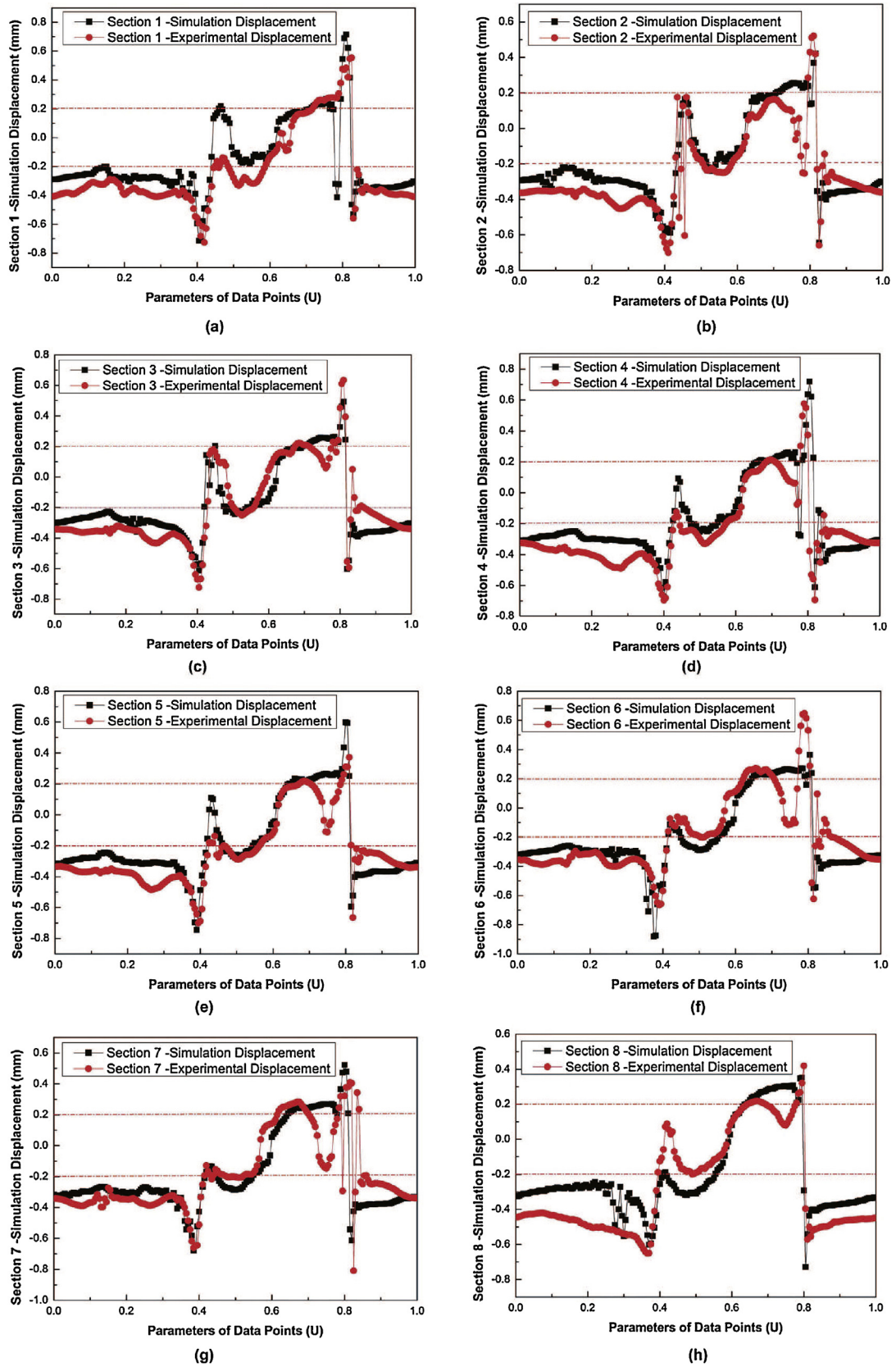


Fig. 15. Comparison of simulated and experimental total displacement fields at the same height.

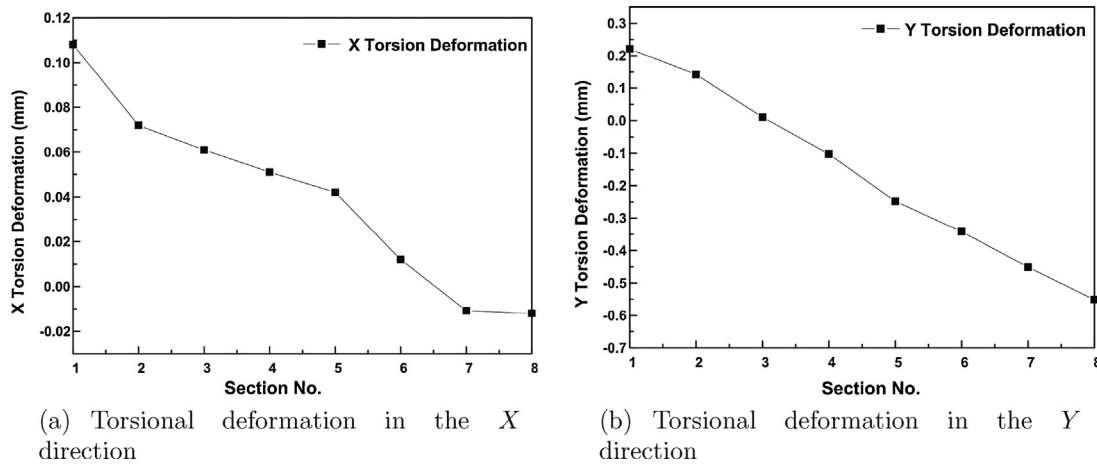


Fig. 16. Schematic of torsional deformation depending on sections of the turbine blade.

hour, then the airfoils of the castings were measured by means of, e.g., a CMM (Brown & Sharpe Global Status 121510, Hexagon Metrology, Qingdao, China) and ATOS (Compact Scan 5M, GOM mbH, Germany).

By analyzing the displacement field of eight groups of cross sections, each point error of the sections can be obtained from an error distribution graph, as shown in Fig. 15. It can be seen that there is a slight difference between the simulation and experimental results. This deviation is primarily due to the calibration error of the thermo-physical parameters of the shell mold material. In this paper, the thermo-physical parameters were chosen from the database of a commercially available FEM software package. Therefore, the calculation of the stress and displacement fields has a deviation owing to the inaccurate thermo-physical parameters and the change of thermal expansion coefficient of the shell mold. However, as illustrated in Fig. 15, the simulated results are in good agreement with the experimental results in aspects of both trend and amount, which proves that the method for predicting the displacement field during the investment casting process is reliable.

#### 4.2. Displacement field decoupling

With the establishment of the displacement field, according to the deformation characteristics decoupling method described in Section 3.1, the torsional deformation can be determined.

Fig. 16(a) and (b) shows the torsional deformation in the X and Y directions for different sections with various heights. For each point lying on the surface of the deformed model, the torsional deformation  $D_{ti}$  can be obtained from Fig. 16 according to the height.

Based on the decoupling method proposed in Section 3.2, the bending deformation characteristics can also be determined, as shown in Fig. 17. For any data point  $P_i$  of the deformed model, the bending deformation (torsional angle) can be obtained from the deformation curve for different cutoff positions.

To verify the modeling of the bending deformation, a cross section was chosen for translation along both X and Y directions for a certain displacement noted as  $T(X)$ ,  $T(Y)$  and then rotated through certain angles in degrees along the Z axis, noted as  $R(Z)$ , as listed in Table 3. If the calculated and given displacement are in a good agreement for both translation and rotation, then the effectiveness of the decoupling method can be proven. The calculated translation and rotation parameters can be determined by the proposed compensation method.

In Table 3,  $X^*$ ,  $Y^*$ , and  $Z^*$  denote the compensation of the bending deformation in the X, Y, and Z directions, respectively. From the calculation results, we can conclude that, based on the proposed

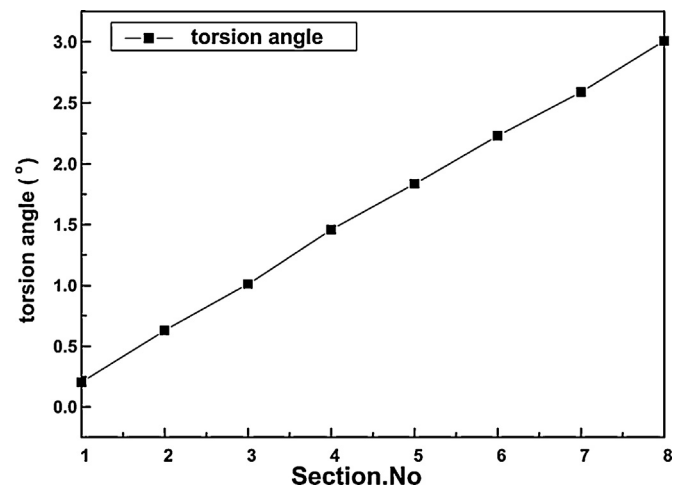


Fig. 17. Variation of the torsion angle with section height.

compensation method, the errors in the translation and rotation parameters were all less than 0.1% with the given deformation parameters. Thus, the deformation characteristics can be precisely decoupled.

In view of the decoupling of bending and torsional deformation from the displacement field, the shrinkage can be determined precisely. As described in Section 2, given the structure of the cross section of the hollow turbine blade, including the regions of DR and NR structures, the wall-thickness distribution can be calculated.

The wall-thickness distributions of sections 3 and 7, shown in Fig. 13, are plotted in Fig. 18(a) and (b), respectively, where the regions I and II represent the leading edge and trailing edge of the turbine blade, respectively, and  $U$  represents the data points parameter of the cross section. It can be seen that the change in the wall thickness of the NR structure follows a uniform trend, whereas the DR structure shows a sharp transition in the wall thickness at the structural change positions. Therefore, the variation characteristics of the wall thickness can be used to determine the structural characteristics and calculate the shrinkage. Based on Eqs. (18) and (19), the nonuniform shrinkage distribution can be obtained. Fig. 19(a) and (b) shows the shrinkage ratio distribution of sections 3 and 7, respectively.

As can be seen in Fig. 19, the shrinkage ratio changes with the parameters of the data points and exhibits a nonuniform distribution, as expected. Further, the shrinkage ratio fluctuates considerably in the intermediate zone of the DR and NR structures,

**Table 3**  
Translation and rotation parameters of cross-section data.

No.	T(X)	T(Y)	R(Z)	X' (mm)	Y' (mm)	Z' (°)
1	0.20	0.20	1.00	0.199720	0.200513	1.00000
2	0.30	0.30	1.10	0.300105	0.299812	1.10102
3	0.40	0.40	1.20	0.400852	0.399802	1.19982
4	0.50	0.50	1.30	0.501427	0.500012	1.30021
5	0.60	0.60	1.40	0.602048	0.599751	1.40082

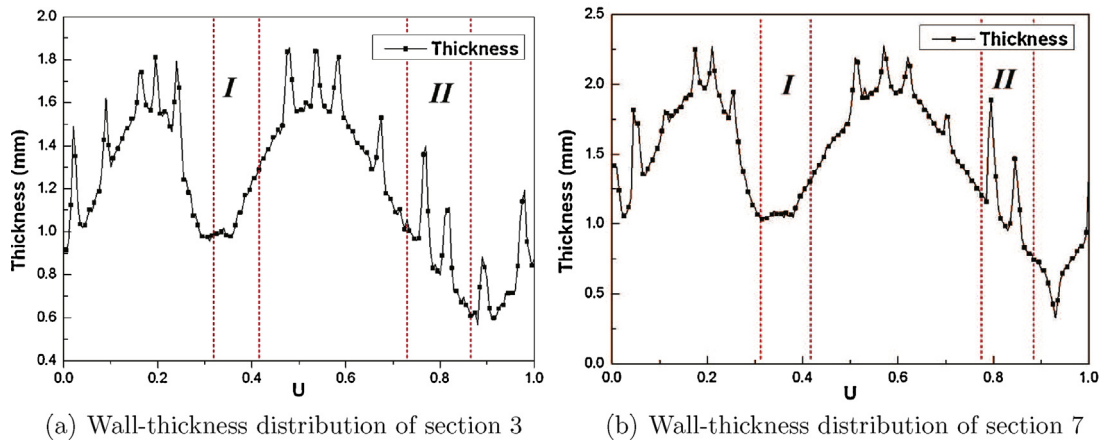


**Fig. 18.** Typical wall-thickness distributions of the hollow turbine blade.

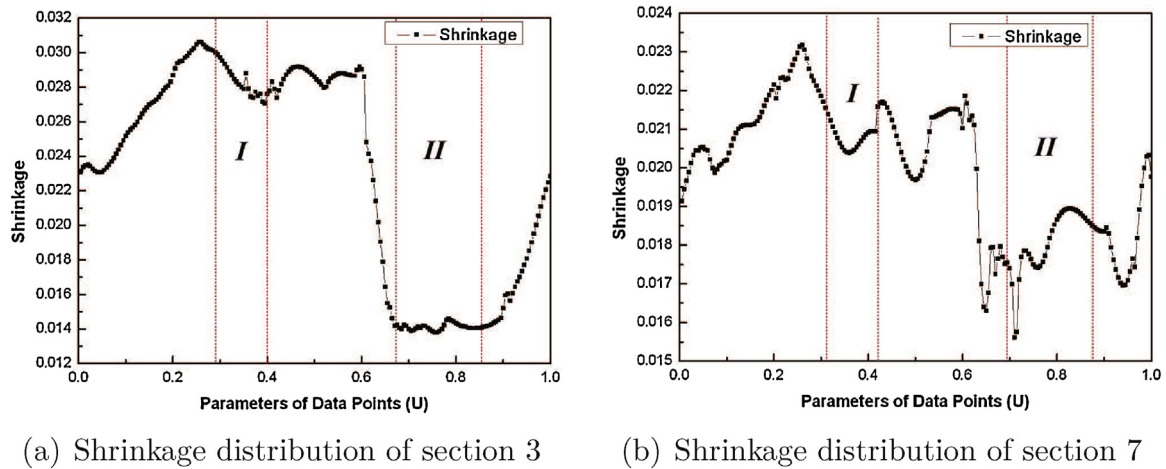


**Fig. 19.** Change in the shrinkage ratio with data-point parameters.

which can be attributed to the change in the wall thickness and the restrained shrinkage from the ceramic core.

#### 4.3. Verification of shrinkage modeling

As mentioned previously, an accurate shrinkage ratio is an essential parameter for determining the appropriate investment cast die profile. Based on the obtained nonuniform shrinkage distribution, the investment casting die profile was designed to verify the accuracy of the shrinkage modeling. We chose an investment cast die that has been actually used for manufacturing the same type of industrial gas turbine blade described in Section 4, but with several modifications to the die profile, as shown in Fig. 20. Since the die profile of the chosen investment cast has been modified by a “trial-and error” method and has been used in industrial application, the contouring error between the die profile designed by using the shrinkage ratio and the die profile of the investment cast die in

actual use can be used for evaluating the accuracy of the shrinkage modeling.

A CMM was used to measure the cross section at the given height  $Z$  ( $Z=60, 70, 80, 90,$  and  $100$  mm) of the cast cavity profile. With the reconstruction of the measurement data and the registration process, the measurement of the investment cast die in actual use was obtained and then compared with that of the die profile determined by the calculated shrinkage at the same height. To evaluate the accuracy of the shrinkage distribution, the cross sections were extracted and dispersed into 200 discrete points in accordance with the number of measurement points of the CMM. The arithmetic mean of the contouring error of each cross section was then calculated.

Fig. 21 shows the normal error histogram of 200 discrete points representing the contouring error. We can conclude that, for 98% of the discrete points on the cross sections, the differences between the die profile designed by the obtained shrinkage model and that of the investment cast die in actual use were all within  $\pm 0.04$  mm.

## investment cast die profile

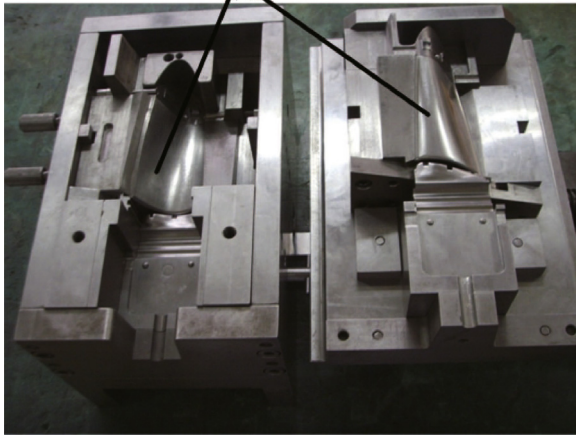


Fig. 20. Images of the investment cast die in actual use.

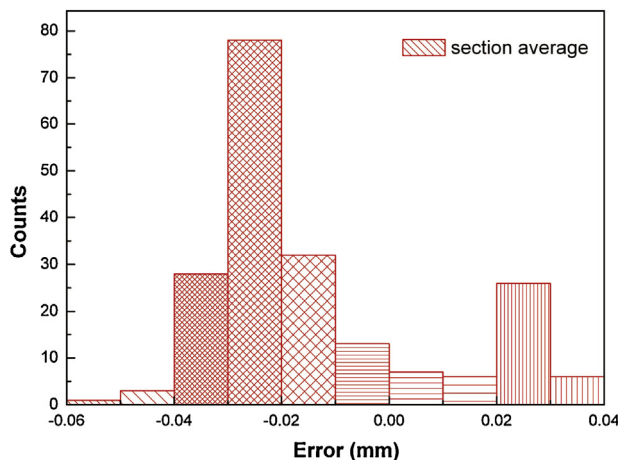


Fig. 21. Histogram of the arithmetic mean of the contouring error between the die profile designed by the obtained shrinkage model and that of the investment cast die in actual use.

The results further confirm that the proposed shrinkage modeling method can be applied to identify the structural characteristics and shrinkage behavior during investment casting, thereby facilitating accurate and reliable investment cast die fabrication.

## 5. Conclusions

The calculation results demonstrated that the method for shrinkage modeling determination can be successfully applied to accurately design the investment cast die profile for hollow turbine blades. The main results of this study can be summarized as follows:

- 1 The proposed structure identification method, including the definitions of the DR and NR structures, the improved threshold algorithm, and the wall-thickness calculation method, was successfully applied to identify the structural characteristics of hollow turbine blades.
- 2 The deformation characteristics of the displacement field were determined by using the deformation characteristics decoupling method; the deformation characteristics of torsion, bending, and shrinkage were established.
- 3 The nonuniform shrinkage distribution obtained by taking into account the structural characteristics of hollow turbine blades

during investment casting as established in this study was verified by comparing the optimized and practical investment cast dies; this may be attributed to the design of the investment cast die for thin-walled hollow turbine blades.

- 4 The shrinkage modeling method proposed is useful for improving the geometrical accuracy of newly developed turbine blades, especially for the newly developed turbine blade model, since the shrinkage generated during the investment casting process cannot be acquired directly.

## Acknowledgments

The authors are grateful for the financial support provided by the PhD Start-up Fund of the Natural Science Foundation of Guangdong Province (2014A030310004), the Major Science and Technology Project between University–Industry Cooperation in Fujian Province (2015H6023), and the China Scholarship Council. The authors are also grateful to Prof. Dinghua Zhang, Prof. Kun Bu, Prof. Wenhui Wang, and Ms. Xiaoyi Ding who offered insightful comments on the manuscript. In addition, the authors would like to thank Northwestern Polytechnical University and the AVIC Xi'an Aero-Engine (Group) Ltd., Xi'an, China, for providing the software and equipment used in this study.

## References

- Afazov, S., Becker, A., Hyde, T., 2011. FE prediction of residual stresses of investment casting in a Bottom Core Vane under equiaxed cooling. *J. Manuf. Process.* 13 (1), 30–40.
- Aveson, J., Tennant, P., Foss, B., Shollock, B., Stone, H., 2013. On the origin of sliver defects in single crystal investment castings. *Acta Mater.* 61, 5162–5171.
- Bergstrom, P., 2015. Evaluation of NURBS surfaces for regular structured parameter values. *J. Comput. Inf. Sci. Eng.* 15 (March (1)), 011005–011005.
- Chattopadhyay, H., 2011. Estimation of solidification time in investment casting process. *Int. J. Adv. Manuf. Technol.* 55 (1–4), 35–38.
- Chvorinov, N., 1940. Theory of solidification of castings. *Giesserei* 27, 177–225.
- Dong, Y., Bu, K., Dou, Y., Zhang, D., 2011a. Determination of interfacial heat-transfer coefficient during investment-casting process of single-crystal blades. *J. Mater. Process. Technol.* 211 (12), 2123–2131.
- Dong, Y., Zhang, D., Bu, K., Dou, Y., Wang, W., 2011b. Geometric parameter-based optimization of the die profile for the investment casting of aerofoil-shaped turbine blades. *Int. J. Adv. Manuf. Technol.* 57 (9–12), 1245–1258.
- Hang, Z., Qingyan, X., Baicheng, L., 2014. Numerical simulation and optimization of directional solidification process of single crystal superalloy casting. *Materials* 7 (3), 1625.
- Jiang, J., Liu, X.Y., 2007. Dimensional variations of castings and moulds in the ceramic mould casting process. *J. Mater. Process. Technol.* 189, 247–255.
- Khan, M.A.A., Sheikh, A.K., 2016. Simulation tools in enhancing metal casting productivity and quality: a review. *Proc. Inst. Mech. Eng. B J. Eng. Manuf.* 1799–1817.
- Li, Z., Xu, Q., Liu, B., 2016. Experimental investigation on recrystallization mechanism of a Ni-base single crystal superalloy. *J. Alloys Compd.* 672, 457–469.
- Liu, C., Jin, S., Lai, X., He, B., Li, F., 2015. Influence of complex structure on the shrinkage of part in investment casting process. *Int. J. Adv. Manuf. Technol.* 77 (5–8), 1191–1203.
- Modukuru, S.C., Ramakrishnan, N., Sriramamurthy, A.M., 1996. Determination of the die profile for the investment casting of aerofoil-shaped turbine blades using the finite-element method. *J. Mater. Process. Technol.* 58 (2–3), 223–226.
- Norouzi, S., Shams, A., Farhangi, H., Darvish, A., 2009. The temperature range in the simulation of residual stress and hot tearing during investment casting. *World Acad. Sci. Eng. Technol.* 58, 283.
- Sabau, A., 2006. Alloy shrinkage factors for the investment casting process. *Metall. Mater. Trans. B* 37 (1), 131–140.
- Wang, D., He, B., Li, F., Sun, B., 2013. Cavity pressure and dimensional accuracy analysis of wax patterns for investment casting. *Mater. Manuf. Process* 28 (June (6)), 637–642.
- Wenlong, L., He, X., Qidong, L., Liping, Z., Zhouping, Y., 2014. Section curve reconstruction and mean-camber curve extraction of a point-sampled blade surface. *PLOS ONE* 9 (12), e115471.
- Xiangdong, Z., Kun, B., Yunyong, C., Yiwei, D., 2012. Research on CMM-based measuring points' sampling and distribution method of blades. *Forg. Stamp. Technol.* 4, 131–135.
- Yunyong, C., Liya, W., Zhenzhen, Z., Dinghua, Z., 2014. Geometric analysis of investment casting turbine blades based on digital measurement data. *China Foundry* 1 (01), 20–27.

- Zhang, D., Jiang, R., Li, J., Wang, W., Bu, K., 2010. [Cavity optimization for investment casting die of turbine blade based on reverse engineering](#). *Int. J. Adv. Manuf. Technol.* 48 (9–12), 839–846.
- Zhao, X., Zhang, C., Yang, B., Li, P., 2011. [Adaptive knot placement using a GMM-based continuous optimization algorithm in B-spline curve approximation](#). *Comput. Aided Des.* 43 (June (6)), 598–604.

**Yiwei Dong** is an Assistant Professor in advanced manufacturing engineering at Xiamen University; Postdoctoral Researcher in materials science engineering at Massachusetts Institute of Technology. Research interests include development of multi-scale computational methods for materials processing by solidification, short laser pulses, machining; investigation of the mechanisms of phase transformations.